

# Utilizing a Paper-Based Platform for Oilfield Applications: Time-Resolved Fluorescence Imaging and Detection of Interwell Chemical Tracers

Bora Yoon, Kiera Y. Tai, Gawain M. Thomas, Hooisweng Ow,\* and Sehoon Chang\*



Cite This: *ACS Omega* 2024, 9, 8239–8246



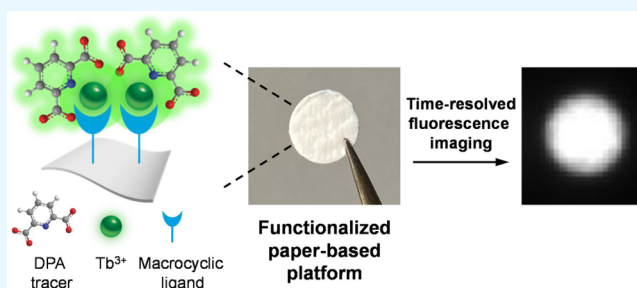
Read Online

ACCESS |

Metrics & More

Article Recommendations

**ABSTRACT:** Chemical tracers are indispensable tools for enhancing reservoir characterization and optimizing production processes in the oil and gas industry. Particularly, interwell water tracers provide key data for efficient water flood management and the improvement of production rates. However, the analysis of these water tracers within reservoir fluids is challenging, requiring laborious separation and extraction steps that often rely on complex instruments and skilled operators. Real-time analysis is especially problematic in remote areas with limited access to well-equipped laboratories. To address these challenges, we introduce a paper-based platform for the time-resolved fluorescence detection of dipicolinic acid (DPA) tracers complexed with terbium ion ( $Tb^{3+}$ ). Our innovation is driven by the need to simplify tracer analysis, make it portable, and enhance accessibility for oilfield applications. By leveraging the unique properties of cyclen-based macrocyclic ligands, we have achieved the stable and sensitive immobilization of  $Tb^{3+}$  on quartz microfilter paper, eliminating the need for extensive laboratory-based procedures. We achieve the stable and sensitive immobilization of  $Tb^{3+}$  on quartz microfilter paper by leveraging the unique properties of cyclen-based macrocyclic ligands. This innovation enables the formation of highly fluorescent, oil-blind, and optically detectable DPA- $Tb^{3+}$  complexes at the paper surface. We visualize and capture these fluorescence signals using an intensified charge-coupled device camera via time gating, effectively suppressing undesirable fluorescence originating from crude oil. The quantification of DPA concentrations is achievable down to 158 ppb ( $9.45 \times 10^{-7}$  M), as confirmed through time-resolved fluorescence microplate reader measurements. We also demonstrate the practicality of our technology by detecting DPA tracers in the presence of crude oil contamination, a common challenge encountered in oil production wells.



## 1. INTRODUCTION

Chemical tracers have become indispensable tools in the oil and gas industry for the purpose of reservoir characterization and production optimization.<sup>1–7</sup> Through the injection of tracers into injection fluids and subsequent monitoring of their presence in adjacent production wells, tracer tests yield a wealth of information pertaining to reservoir well connectivity and heterogeneity. Recent advancements in tracer technology have significantly accelerated the process of data acquisition and analysis. Innovations such as microencapsulation techniques<sup>8</sup> and the utilization of fluorescent-based tracers for near-real-time drilling depth monitoring<sup>9</sup> have enhanced tracer applications in reservoir engineering. These methods facilitate more rapid and accurate assessments of the reservoir conditions. Notably, interwell water tracers offer valuable insights that enable efficient water flood management and enhanced production rates with more precise predictions.<sup>1–3</sup> However, the analysis of these water tracers in reservoir fluid often necessitates time-consuming separation and extraction procedures to eliminate solution interference, requiring

sophisticated instruments operated by skilled professionals. For instance, while industrial conventional fluorobenzoic acid-based tracers exhibit exceptional transport behavior with low detection limits, their analysis demands intricate sample preparations, including chemical derivatization using hazardous chemicals, to enable their detection using analytical techniques, i.e., gas chromatography-tandem mass spectrometry.<sup>1,10</sup> This poses significant challenges in implementing tracer analysis systems, especially in remote regions with limited access to well-equipped laboratories.

To address these challenges, paper-based platforms have emerged as a practical solution. They have demonstrated their effectiveness in various fields including environmental

**Received:** November 8, 2023

**Revised:** January 18, 2024

**Accepted:** January 24, 2024

**Published:** February 6, 2024



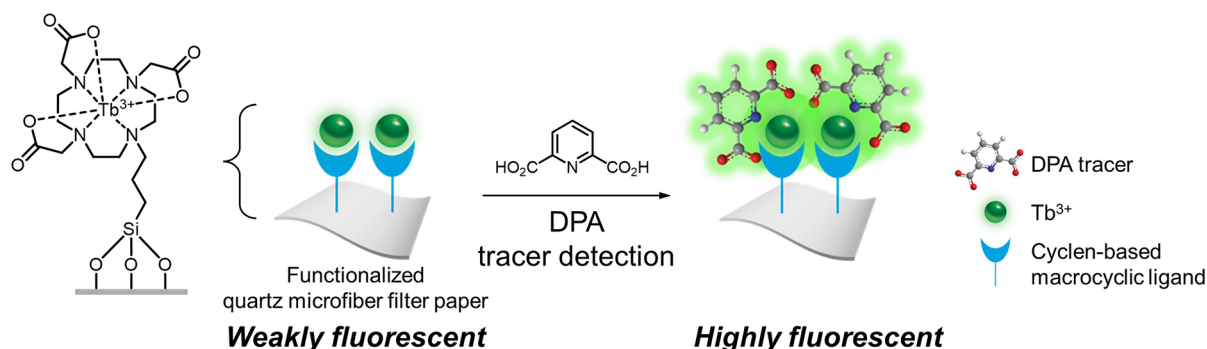


**Figure 1.** Schematic illustration of surface functionalization for interwell chemical tracer detection on a quartz microfiber filter paper substrate.

monitoring, healthcare diagnostics, food safety, and water quality assessment.<sup>11–14</sup> These applications have highlighted the potential of paper-based platforms to provide rapid results through low-cost, portable, and user-friendly devices while minimizing the need for sample and reagent consumption. By leveraging the advantages of paper-based platforms, engineers in the oilfield can conveniently obtain tracer analysis without the need for bulky laboratory setups. Moreover, the compact nature of these platforms facilitates their transportation through challenging oilfield environments.

In our previous efforts aimed at developing interwell water tracers for oilfield applications, we have successfully developed optically detectable tracer systems that utilize lanthanide chelate complexes.<sup>15–20</sup> In particular, dipicolinic acid (DPA) and its derivatives have been employed to monitor the flow of water within oil reservoirs. These tracers serve as ligands for terbium ions ( $Tb^{3+}$ ), facilitating efficient sensitization of  $Tb^{3+}$  through energy transfer upon complex excitation, leading to a high degree of lanthanide luminescence.<sup>21–26</sup> Importantly, the resulting complex demonstrates longer lifetime luminescence, which effectively filters out any background fluorescence signals originating from crude oil, enabling ultratrace-level detectability of the tracers. In addition, DPA-based tracers exhibit high stability in challenging high-salinity, high-temperature subsurface environments.<sup>15–17</sup> They also demonstrate minimal retention to carbonate reservoir rock matrices, allowing them to efficiently traverse through interconnected pore networks.

Expanding upon the benefits presented by lanthanide-based chemistry for oilfield tracers and harnessing the potential of paper-based platforms in this context, our current study introduces a chemically versatile paper-based platform specifically designed for the time-resolved fluorescence detection of DPA- $Tb^{3+}$  complexes at the paper surface. In the proposed platform in Figure 1, DPA tracers react with  $Tb^{3+}$  that is bound to the surface of a quartz microfiber filter paper substrate, resulting in the formation of a highly fluorescent, oil-blind, and optically detectable complex. To enhance the robustness and sensitivity of the detection process, we have first introduced cyclen-based macrocyclic chelating agents to the paper surface via organosilanization. These macrocyclic agents possess an exceptional affinity for  $Tb^{3+}$ ,<sup>27–31</sup> enabling the stable and secure immobilization of  $Tb^{3+}$  at the paper surface through the formation of chelates. This crucial step establishes a reliable platform that facilitates the desired interaction between  $Tb^{3+}$  and DPA tracers. To capture and visualize the fluorescence signals before and after the detection of DPA tracers, an intensified charge-coupled device (ICCD)

camera was utilized, which can effectively suppress any undesirable fluorescence originating from crude oil via time-gating. Through fluorescence imaging of the functionalized substrates, we investigated the detection limits of DPA tracers on the functionalized paper platform by varying concentrations of DPA tracers in water solutions. Finally, we demonstrated the time-resolved fluorescence imaging of DPA at trace levels in water solutions in the presence of crude oil. This type of contamination is commonly encountered in field applications when tracers are recovered in oil production wells. The ability to accurately detect and analyze fluorescence signals in the presence of such crude oil contaminants is crucial for the practical application of this technology in oilfield environments.

## 2. EXPERIMENTAL SECTION

**2.1. Materials.** All chemicals and reagents were purchased from Sigma-Aldrich and used without additional purification unless noted otherwise. 1,4,7,10-Tetraazacyclododecane-1,4,7-tris(*t*-butyl acetate) was purchased from AmBeed. Tri-*tert*-butyl 2,2',2''-(10-(3-(trimethoxysilyl)propyl)-1,4,7,10-tetraazacyclododecane-1,4,7-triyl)triacetate (DO3A-*t*Bu-TMS) was synthesized according to a previously reported method.<sup>32,33</sup> Deuterated solvents for NMR spectroscopy were purchased from Cambridge Isotope Laboratories, Inc. Quartz microfiber filters (Grade QM-A) were purchased from Cytiva. 3-Iodopropyltrimethoxysilane was purchased from Gelest.

**2.2. Characterization.**  $^1H$  and  $^{13}C$  NMR spectra were acquired by Bruker Ascend 500 spectrometer at 500 and 126 MHz for  $^1H$  and  $^{13}C$ , respectively. ATR-FTIR spectra were obtained using a Thermo Scientific Nicolet iS50R FTIR with a Ge crystal for ATR. Oxygen plasma treatment of paper surface employed using a plasma etch system PE-50 (Plasma Etch, Inc.). The static water contact angles on the surfaces were measured using a Ramé-Hart goniometer (model 250) by vertical deposition of 5  $\mu L$  water droplets. Scanning electron microscope (SEM) images were obtained using a JEOL JSM-7100F SEM at an accelerating voltage of 15 kV. The energy-dispersive X-ray spectroscopy (EDS) was measured using Oxford Instruments EDS system attached to SEM. The time-resolved images were acquired using an ICCD camera (PI-MAX 4:1024B/EM, Teledyne Princeton Instruments). The samples were illuminated by a pulsed light source using a UV LED (Thorlabs). A diffuser glass (200 grit, Thorlabs) was placed in front of the LED to ensure uniform illumination of the samples by the LED light. Additionally, a green lens filter (Edmund Optics) was installed in front of the camera objective lens to gather emission wavelengths centered around 540 nm

for Tb<sup>3+</sup>. A 96-well microplate (Thermo Scientific Nunc MicroWell 96-Well, black) with a polystyrene film at the bottom was utilized to minimize scattered UV light from the substrate and ensure uniform spacing for imaging. LightField data acquisition software (Teledyne Princeton Instruments) was used to control and process images captured by the camera. Additional fluorescence intensity data was obtained using a BioTek Synergy H1 microplate reader.

**2.3. Synthesis of the Macrocyclic Ligand.** Tri-*tert*-butyl 2,2',2''-(10-(3-(trimethoxysilyl)propyl)-1,4,7,10-tetraazacyclododecane-1,4,7-triyl)triacetate was synthesized according to a previously reported method with slight modifications.<sup>32,33</sup> 1,4,7-Tris(*tert*-butoxycarbonylmethyl)-1,4,7,10-tetraazacyclododecane (DO3A-*t*-Bu, 1.00 g, 1.94 mmol) and anhydrous potassium carbonate (0.54 g, 3.88 mmol) were added to a round-bottom flask with a stir bar. After the solution in anhydrous acetonitrile (50 mL), 3-iodopropyltrimethoxysilane (0.84 g, 2.91 mmol) was added, and then the mixture was heated to 80 °C and refluxed for 48 h. After the mixture was cooled to room temperature, the white precipitate was removed by filtration. The filtrate was concentrated in vacuo to yield a light yellow solid, which was used in the following surface functionalization step without further purification (quantitative yield). <sup>1</sup>H NMR (500 MHz, chloroform-*d*) δ 3.43 (s, 9H, Si-(OCH<sub>3</sub>)<sub>3</sub>), 3.27–1.90 (m, 24H, CH<sub>2</sub>C=O, N-(CH<sub>2</sub>)<sub>2</sub>-N), 1.71–1.50 (m, 2H, CH<sub>2</sub>-CH<sub>2</sub>-Si), 1.33 (d, *J* = 16.2 Hz, 27H, *t*-Bu), 0.41 (t, *J* = 8.3 Hz, 2H, CH<sub>2</sub>-CH<sub>2</sub>-Si). <sup>13</sup>C NMR (126 MHz, chloroform-*d*) δ: 172.28, 172.05, 82.04, 81.98, 56.90, 56.76, 56.43, 54.44, 50.38, 50.34, 50.16, 50.12, 27.79, 27.77, 16.44, and 6.67. <sup>29</sup>Si NMR (99 MHz, chloroform-*d*) δ -42.51. FT-IR (ATR) μ 2974, 2936, 2836, 2820 (C-H), 1725 (C=O), 1155 (C-O), and 1098 (Si-O) cm<sup>-1</sup>.

**2.4. Surface Functionalization.** Quartz microfiber filter paper slides, approximately 75 × 25 mm in size, were treated with oxygen plasma for 1 min. Subsequently, these paper substrates were immersed in a solution of synthesized DO3A-*t*-Bu-TMS in dry toluene at room temperature for 17 h. The ratio employed was 0.1 mmol of DO3A-*t*-Bu-TMS per slide of quartz paper with 60 mL of toluene used to fully submerge each paper slide. Following the organosilanization, the paper substrates underwent thorough washing with pure toluene and were then dried using N<sub>2</sub>. The next step involved the hydrolysis of the *tert*-butyl ester groups. The paper substrates were soaked in a 1:3 mixture of trifluoroacetic acid (TFA) and dichloromethane (DCM) for 3 h at room temperature. Following hydrolysis, the substrates were washed with DCM and dried using N<sub>2</sub>. In the final step, the papers were immersed in a TbCl<sub>3</sub>·6H<sub>2</sub>O solution with a total of 60 mL of water and 0.1 mmol of lanthanide added per slide. The pH of the solution was adjusted to fall within the range 6.5–7.0 by adding dilute NaOH or HCl drops. The papers were allowed to soak in the TbCl<sub>3</sub> solution overnight at 60 °C. The final functionalized papers were washed with water and dried using compressed air.

## 2.5. Imaging Procedure for Tracer Detection.

**2.5.1. General Imaging Procedures for Tracer Detection.** 2,6-Pyridinedicarboxylic acid (DPA) solutions with various concentrations were prepared in DI water via stepwise dilution, ranging from 1 ppb to 100 ppm (5.98 × 10<sup>-9</sup> to 5.98 × 10<sup>-4</sup> M). Small circular samples with a diameter of 6 mm were excised from the functionalized quartz paper using a hole punch. Samples with uniform background fluorescence were identified using the time-resolved camera and assembled into

test groups. These grouped samples were subsequently immersed in 1 mL of DPA solutions with varying concentrations for 30 min. Then, the samples were placed in a 96-well microplate to maintain their positions evenly spaced. Each sample was wet with 40 μL of deionized water before the microplate was inverted within the camera setup, enabling imaging through the clear plastic well bottoms. The ICCD camera was positioned vertically, pointing downward, with the sample stage placed parallel to the tabletop. The images were acquired using 300 on-CCD accumulations and signal amplification of 50. The gating was set to a repetitive cycle with delay of 500 μs with a full measurement window of 1.2 ms. Sample illumination was employed using a pulsed UV LED excitation at 300 nm with 360 μs pulse width. For each data collection, we captured 50 frames, and the resultant fluorescence intensity was determined by averaging these frames. For background noise reduction, a reference background was acquired with the LED turned off, used for background subtraction during data analysis using the LightField data acquisition software.

**2.5.2. Tracer Detection Using a Microplate Reader.** A 276 nm λ<sub>ex</sub>/495 nm λ<sub>em</sub> filter cube was used to collect the fluorescence intensity data from the BioTek Synergy H1 microplate reader. The samples were placed on a 96-well microplate with a polystyrene film at the bottom. The time-resolved fluorescence signals at 495 nm were recorded upon excitation wavelength at 276 nm with 100 μs of delay and 300 μs of gate time. The measurement height was 1 mm with 135 of fluorescence signal gain.

## 3. RESULTS AND DISCUSSION

A cyclen-based macrocyclic ligand, 1,4,7,10-tetraazacyclododecane-1,4,7,10-tetraacetic acid and their derivatives have been extensively studied for lanthanide complexation because of their high affinity toward the target lanthanide ions including Tb<sup>3+</sup>.<sup>27–31</sup> The stability of the binding is attributed to the presence of four nitrogen atoms within the cyclen ring, which establish robust binding sites for lanthanide ions. Additional carboxylic acid groups further enhance the binding affinity, thereby improving the sensitization efficiency for lanthanide ions. Furthermore, it can be readily subjected to synthetic elaboration to achieve structural versatility because of the inherent amine functionality. In order to demonstrate these desired properties on a paper-based surface, we have synthesized tri-*tert*-butyl 2,2',2''-(10-(3-(trimethoxysilyl)propyl)-1,4,7,10-tetraazacyclododecane-1,4,7-triyl)triacetate (DO3A-*t*-Bu-TMS) as shown in Figure 2. This was accomplished by introducing a pendant trimethoxysilyl group using 3-iodopropyltrimethoxysilane into a precursor starting reagent of 1,4,7-tris(*tert*-butoxycarbonylmethyl)-1,4,7,10-tetraazacyclododecane (DO3A-*t*-Bu), employing a previously reported method with slight modifications.<sup>32,33</sup> The incorporation of the pendant trimethoxysilyl group facilitates the

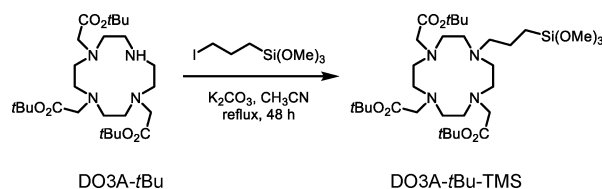
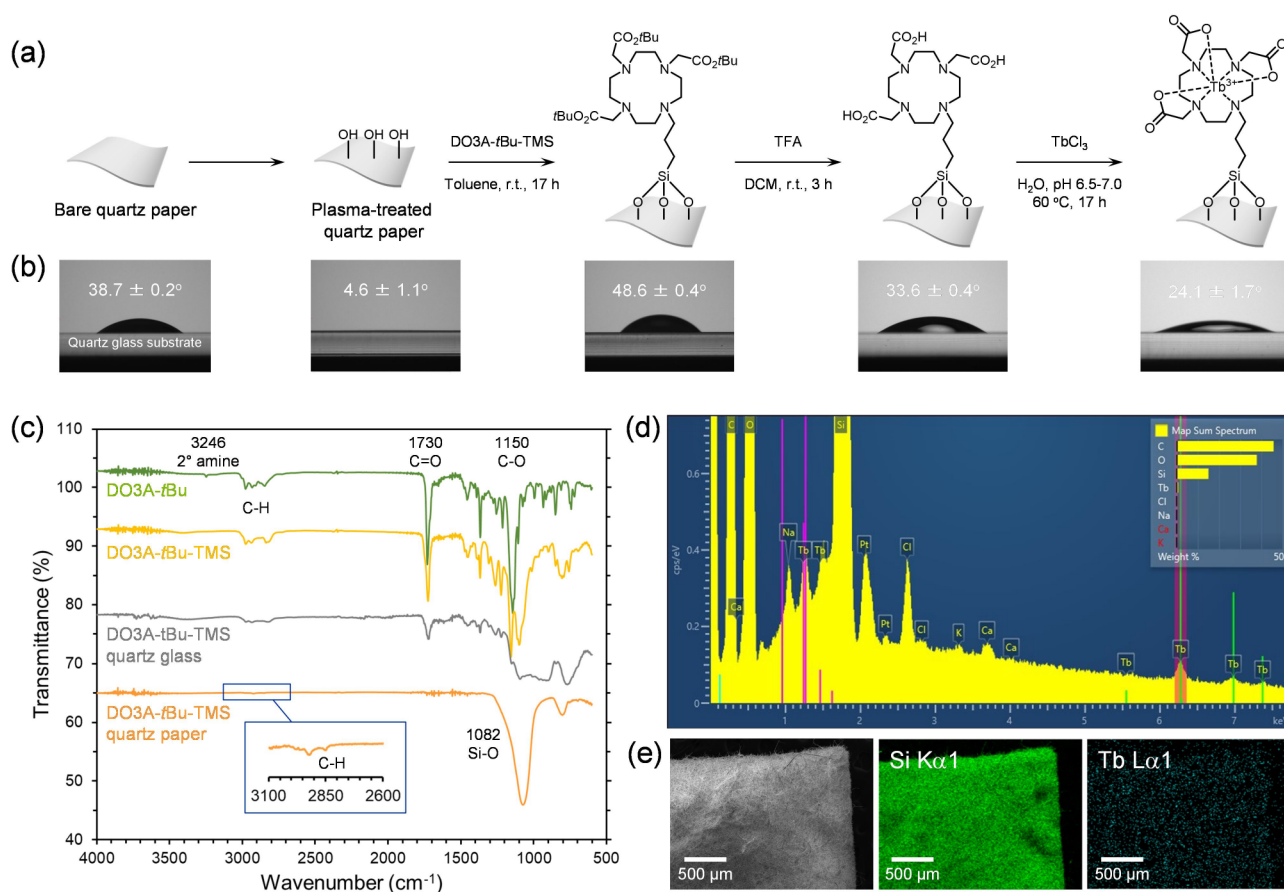


Figure 2. Synthetic scheme of DO3A-*t*-Bu-TMS.



**Figure 3.** (a) Schematic illustration outlining the individual steps of the surface functionalization process. (b) Water contact angle measurements of each step of the surface functionalization on a quartz glass substrate. (c) ATR-FTIR spectra of the DO3A-*t*Bu, DO3A-*t*Bu-TMS, a quartz glass functionalized with DO3A-*t*Bu-TMS, and a quartz microfiber filter paper functionalized with DO3A-*t*Bu-TMS. (d) EDS spectrum of the quartz paper surface functionalized with Tb<sup>3+</sup> chelated to the macrocyclic ligand. Terbium peaks are highlighted in pink. (e) SEM image of the functionalized quartz paper surface and EDS maps of the corresponding area for silicon and terbium.

subsequent organosilanization process with surface hydroxyl groups present on the paper-based substrate, thereby anchoring the macrocyclic ligand onto the paper surface.

Figure 3a provides a schematic illustration outlining the individual steps of the surface functionalization process. To create a surface functionalized with Tb<sup>3+</sup> chelated to the cyclen-based ligand, anchored on a paper surface for DPA detection, the initial step involved treating a quartz microfiber filter paper substrate with oxygen plasma to introduce hydroxyl groups onto the surface. A quartz microfiber filter paper substrate was selected for this study due to its relatively lower fluorescence background under UV light excitation compared to other types of filter papers, which is desirable for the sensitive detection of DPA tracers. The substrate was then immersed in a solution of DO3A-*t*Bu-TMS in dry toluene at room temperature for 17 h, allowing effective ligand anchoring via organosilanization. Subsequently, the substrate underwent hydrolysis of *tert*-butyl ester groups through immersion in a 1:3 mixture of TFA and DCM for 3 h at room temperature. Lastly, the substrate was enriched with Tb<sup>3+</sup> through the formation of chelates with the surface-anchored ligands during an overnight immersion within a TbCl<sub>3</sub> solution at 60 °C. Each step of the surface functionalization was confirmed through water contact angle measurements on a quartz glass substrate treated with the same functionalization procedure (Figure 3b). It should be noted that analyzing the surface of the functionalized quartz

paper using water contact angle measurements posed challenges due to its tendency to absorb water droplets, rendering accurate measurement unattainable. On the initial pristine quartz glass substrate, a 5- $\mu$ L water droplet displayed a contact angle of  $38.7 \pm 0.2^\circ$ . Following oxygen plasma treatment, the droplet exhibited immediate spreading upon contact with the substrate with a contact angle of  $4.6 \pm 1.1^\circ$ , indicating a significant enhancement in surface hydrophilicity. During the organosilanization with DO3A-*t*Bu-TMS, the wettability of the surface was altered, resulting in an increased contact angle of  $48.6 \pm 0.4^\circ$  due to an increased hydrophobicity stemming from the hydrophobic *tert*-butyl ester groups on the macrocyclic ligand. This observation confirms its successful incorporation on the surface. Subsequently, through hydrolysis using TFA, the *tert*-butyl ester groups were converted into carboxylic acid groups. This conversion corresponded to an observed increase in surface hydrophilicity, evident in a contact angle of  $33.6 \pm 0.4^\circ$ . Finally, following the introduction of Tb<sup>3+</sup>, the contact angle experienced a further decrease to  $24.1 \pm 1.7^\circ$ , likely attributed to the introduction of charged ions. The changes in surface hydrophobicity align with the expectation at each step in the functionalization process.

The characterization of the functionalized surface on a quartz microfiber filter paper substrate was performed by attenuated total reflection-Fourier transform infrared (ATR-FTIR) spectroscopy (Figure 3c). The macrocyclic ligand

DO3A-*t*Bu-TMS and its precursor compound DO3A-*t*Bu were first characterized for comparison with the peaks observed on the quartz glass and paper surface treated with DO3A-*t*Bu-TMS. DO3A-*t*Bu exhibited a distinctive N–H stretching band at  $3246\text{ cm}^{-1}$ , indicative of the secondary amine, which became absent after its reaction with 3-iodopropyltrimethoxysilane, leading to the formation of DO3A-*t*Bu-TMS. Both DO3A-*t*Bu and DO3A-*t*Bu-TMS showed characteristic *tert*-butyl ester bands in their spectra, with a C=O stretching band at  $1730\text{ cm}^{-1}$  and a C–O stretching vibration at around  $1150\text{ cm}^{-1}$ . Additionally, the broad C–H stretching modes attributed to both the *tert*-butyl groups and the CH<sub>2</sub> groups were observed in the range of  $2844\text{--}2978\text{ cm}^{-1}$ .<sup>34</sup> We then analyzed quartz glass and a quartz microfiber filter paper substrate functionalized with DO3A-*t*Bu-TMS. In the case of the functionalized quartz glass, the anticipated C=O and C–H stretching bands were clearly discernible, providing evidence of DO3A-*t*Bu-TMS immobilization on the quartz glass surface via organosilanization. However, it is noteworthy that the inherently rough and fibrous surface of quartz paper substrate posed challenges in detecting functional groups. The C–H stretching modes observed in the  $2853\text{--}2980\text{ cm}^{-1}$  range in the spectrum of functionalized quartz paper indicated the presence of surface-anchored DO3A-*t*Bu-TMS on the paper surface. However, considerable noise signals from the pristine quartz paper emerged between  $1500$  and  $2000\text{ cm}^{-1}$ , making the differentiation of the C=O stretching band from the *tert*-butyl ester group challenging. Additionally, the distinction of the *tert*-butyl ester C–O band proved to be challenging due to the substantial overlap with the extensive Si–O band from the quartz paper.

The progression of the Tb<sup>3+</sup> binding to the macrocyclic ligand anchored on the paper surface after TFA hydrolysis was confirmed by SEM equipped with EDS to determine Tb<sup>3+</sup> composition on the functionalized surface as shown in Figure 3d. The EDS spectrum distinctly presents the characteristic La X-ray emission peak for Tb<sup>3+</sup> at around 6.27 keV, thereby confirming the presence of Tb<sup>3+</sup> chelates at the paper surface.<sup>33,35</sup> The morphology of the functionalized paper shows a typical rough fibrous surface (Figure 3e). During the EDS signal mapping of the corresponding areas for silicon and terbium, a uniform distribution of Tb<sup>3+</sup> across the substrate surface was clearly observable.

To further investigate the effect of surface functionalization for Tb<sup>3+</sup> incorporation via chelate formation with the surface-anchored ligands, time-resolved fluorescence imaging was employed by using an ICCD camera with a 500 μs gate delay upon pulsed UV LED excitation at 300 nm. The camera was positioned vertically and oriented downward onto a horizontal sample stage parallel to the ground (Figure 4a). A control sample was prepared by immersing pristine quartz paper into a TbCl<sub>3</sub> solution at 60 °C overnight. Under the time-resolved camera, the functionalized quartz paper exhibited fluorescence nearly four times higher than the nonfunctionalized paper (Figure 4b). Since both substrates underwent immersion in a Tb<sup>3+</sup> solution, followed by thorough washing, the significantly increased fluorescence from the functionalized substrate suggests effective chemical binding of Tb<sup>3+</sup> to the surface. It is important to note that while Tb<sup>3+</sup> itself has weak fluorescence, this fluorescence becomes evident when contrasted with the control sample under observation by the time-resolved camera. This comparison is possible due to

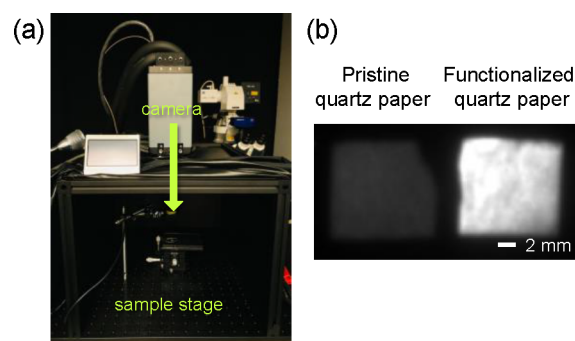


**Figure 4.** (a) Configuration of time-resolved fluorescence imaging using an ICCD camera. (b) Comparison of Tb<sup>3+</sup> fluorescence signals on pristine and functionalized quartz paper by using the time-resolved camera.

the relative fluorescence being imaged against the almost negligible fluorescence of the nonfunctionalized substrate.

To demonstrate DPA tracer detection using our paper-based platform, small circular samples were obtained from functionalized quartz paper via a 6-mm diameter hole punch (Figure 5a). Since Tb<sup>3+</sup> background fluorescence signals could vary between substrates, samples exhibiting consistent and homogeneous background fluorescence were initially identified using the time-resolved camera and grouped for equitable comparison before DPA detection. The grouped samples were subsequently immersed in 1 mL of DPA solutions with varying concentrations for 30 min and then securely positioned within a 96-well microplate to ensure uniform spacing for imaging. Each sample was wetted with 40 μL of deionized water before the microplate was inverted onto the sample stage for imaging through the clear plastic well bottoms, with the added water enhancing even adhesion to the wells. Fluorescence images of the quartz papers treated with different concentrations of DPA were acquired after pulsed excitation at 300 nm using a UV LED with 360 μs pulse width, which excites the DPA complexed with the surface-anchored Tb<sup>3+</sup>. Following a 500 μs delay upon switching off the LED, the ICCD camera captured the Tb<sup>3+</sup> emission from the excited complexes with a full measurement window of 1.2 ms. A diffuser was employed to ensure uniform illumination of the samples by the LED light. Additionally, a green lens filter was integrated to gather emission wavelengths centered around 540 nm for Tb<sup>3+</sup>. In Figure 5b, the fluorescence intensity increases as the concentration of DPA increases. The control quartz paper, which has incorporated Tb<sup>3+</sup> but no DPA treatment, displays negligible fluorescence when compared to that of the DPA-treated quartz papers. The fluorescence of the quartz paper reacted with 50 ppb ( $2.99 \times 10^{-7}\text{ M}$ ) of DPA is distinctly discernible from the control sample. This could facilitate field engineers in detecting tracers from oil field-produced water through a simple visual inspection using the camera. The fluorescence intensity data were extracted from each captured image using LightField data acquisition software and plotted against the DPA concentration, revealing an approximately linear correlation with an *r*-squared value of 0.90 (Figure 5c). While the camera allows the optical detection of DPA presence at concentrations as low as tens of ppb, challenges emerge from the autoscaling feature and arbitrary fluorescence intensity units of the camera as well as variations in background fluorescence among samples. These factors

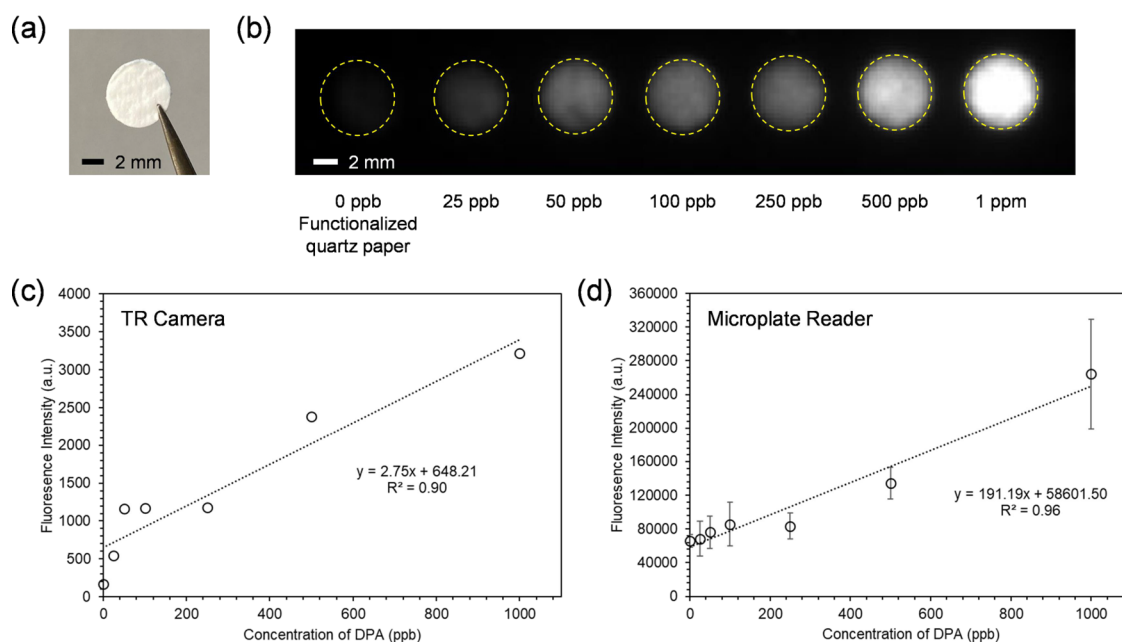


**Figure 5.** (a) Photograph of a functionalized circular quartz paper. (b) Time-resolved fluorescence camera image of DPA detection at varying concentrations and (c) their fluorescence intensity extracted from each captured image using LightField data acquisition software plotted against DPA concentration. The corresponding molar concentrations for the given values in ppb are as follows: 25 ppb ( $1.50 \times 10^{-7}$  M), 50 ppb ( $2.99 \times 10^{-7}$  M), 100 ppb ( $5.98 \times 10^{-7}$  M), 250 ppb ( $1.50 \times 10^{-6}$  M), 500 ppb ( $2.99 \times 10^{-6}$  M), and 1 ppm ( $5.98 \times 10^{-6}$  M). (d) Averaged time-resolved fluorescence intensities of three sets of samples treated with varying concentrations of DPA recorded on a microplate reader.

collectively hinder direct comparisons across different grouped samples.

Further confirmation of DPA detection on the functionalized paper platform was achieved through time-resolved fluorescence measurements using a microplate reader. Three sets of samples, each consisting of seven circular quartz papers functionalized with  $\text{Tb}^{3+}$  bound to the surface macrocyclic ligand and exhibiting consistent and uniform background fluorescence within their respective groups, were subjected to DPA detection. They were immersed in DPA solutions with varying concentrations, and their time-resolved fluorescence was subsequently recorded using a microplate reader. The fluorescence signals at 495 nm were recorded upon excitation at 276 nm with a 100  $\mu\text{s}$  delay and 300  $\mu\text{s}$  gate time. This delay time allows for the suppression of crude oil fluorescence signals, as their fluorescence lifetimes are relatively shorter compared to those of the DPA- $\text{Tb}^{3+}$  complex. The averaged time-resolved fluorescence intensities upon detecting DPA concentrations ranging from 25 ppb to 1 ppm ( $1.50 \times 10^{-7}$  to  $5.98 \times 10^{-6}$  M) are presented in Figure 5d. The background  $\text{Tb}^{3+}$  signal from the control quartz paper exhibited a slightly discernible fluorescence intensity in comparison to the measurement acquired by an ICCD camera, where no measurable fluorescence was observed from the control sample when contrasted with the brighter images that detected higher concentrations of DPA. The limit of detection in concentration was calculated as  $(\text{mean}_b + 3\sigma_b - a)/b$ , where  $\text{mean}_b$  represents the average fluorescence intensity of three measurements of the control quartz paper,  $\sigma_b$  is the standard deviation for the control,  $a$  is the intercept of the linear regression, and  $b$  denotes the slope of the linear regression. Based on the microplate reader measurements, the calculated limit of detection for DPA was 158 ppb ( $9.45 \times 10^{-7}$  M).

To demonstrate the practical application of our time-resolved imaging technology in the proposed paper-based

platform, we conducted imaging on samples immersed in 25 ppb ( $1.50 \times 10^{-7}$  M) of DPA in water containing crude oil (Figure 6). Such contamination scenarios are plausible in field

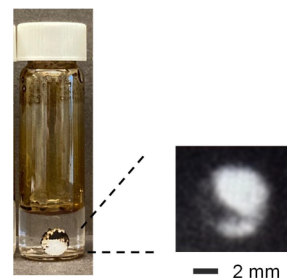


**Figure 6.** Photograph of a functionalized circular quartz paper immersed in 25 ppb ( $1.50 \times 10^{-7}$  M) of a DPA solution containing crude oil and its time-resolved fluorescence camera image.

settings during the recovery of tracers from oil production wells. We found that while the presence of crude oil on the paper obscured the fluorescence signal from the  $\text{Tb}^{3+}$ -complexed tracer, crude oil itself did not contribute to the measured signal, likely due to the effective background fluorescence filtration provided by oil-blind, time-resolved imaging. In practical oilfield applications, note that the presence of high salt concentrations in produced water may hinder the direct complexation of DPA with  $\text{Tb}^{3+}$ . To address this, a preprocessing step, such as solid-phase extraction, can be employed to preconcentrate DPA tracers and remove salts from the produced water, ensuring effective complexation and accurate detection using the paper-based platform.<sup>15,16</sup> This technique can also be adapted for applications similar to pH strips, where various substrates soaked in known tracer concentrations are imaged alongside an unknown sample,

enabling rapid and semiquantitative analysis of unknown samples for tracer detection.

#### 4. CONCLUSIONS

In conclusion, we demonstrated an innovative paper-based platform for the time-resolved fluorescence detection of DPA tracers complexed with  $Tb^{3+}$ , with a particular focus on its applicability within the oil and gas industry. The surface functionalization of quartz microfiber filter paper with cyclen-based macrocyclic ligands successfully anchored  $Tb^{3+}$  to the quartz paper surface through the formation of chelates, enabling stable and sensitive DPA- $Tb^{3+}$  complex formation on the paper surface. Time-resolved fluorescence imaging, aided by an ICCD camera, was used to capture and visualize the fluorescence signals from the DPA- $Tb^{3+}$  complexes on the paper surface. This technique effectively suppresses unwanted fluorescence signals originating from crude oil or other contaminants. Based on microplate reader measurements, the quantification of DPA concentrations is achievable down to 158 ppb ( $9.45 \times 10^{-7}$  M). We also demonstrated the practicality of our technology by detecting DPA tracers in the presence of crude oil contamination. The developed technology is noteworthy for its versatility, as it extends beyond DPA- $Tb^{3+}$  complexes, opening possibilities for the exploration of optical sensors based on various lanthanides. By harnessing the inherent benefits of paper-based platforms, our approach offers a portable, cost-effective, and user-friendly solution for efficiently detecting DPA tracers in challenging oilfield environments.

#### AUTHOR INFORMATION

##### Corresponding Authors

**Hooisweng Ow** – Aramco Americas: Aramco Research Center, Cambridge, Massachusetts 02139, United States; [orcid.org/0000-0002-9196-5814](https://orcid.org/0000-0002-9196-5814); Email: [hooisweng@gmail.com](mailto:hooisweng@gmail.com)

**Sehoon Chang** – Aramco Americas: Aramco Research Center, Cambridge, Massachusetts 02139, United States; [orcid.org/0000-0002-8007-4354](https://orcid.org/0000-0002-8007-4354); Email: [sehoon.chang@aramcoamericas.com](mailto:sehoon.chang@aramcoamericas.com)

##### Authors

**Bora Yoon** – Aramco Americas: Aramco Research Center, Cambridge, Massachusetts 02139, United States; [orcid.org/0000-0003-1338-7841](https://orcid.org/0000-0003-1338-7841)

**Kiera Y. Tai** – Aramco Americas: Aramco Research Center, Cambridge, Massachusetts 02139, United States

**Gawain M. Thomas** – Aramco Americas: Aramco Research Center, Cambridge, Massachusetts 02139, United States

Complete contact information is available at:

<https://pubs.acs.org/10.1021/acsomega.3c08902>

##### Author Contributions

The manuscript was written through contributions of all authors. All authors have given their approval to the final version of the manuscript.

##### Notes

The authors declare no competing financial interest.

#### REFERENCES

- (1) Serres-Piole, C.; Preud'homme, H.; Moradi-Tehrani, N.; Allanic, C.; Jullia, H.; Lobinski, R. Water tracers in Oilfield Applications: Guidelines. *J. Petrol. Sci. Eng.* **2012**, *98–99*, 22–39.
- (2) Serres-Piole, C.; Commarieu, A.; Garraud, H.; Lobinski, R.; Preud'homme, H. New Passive Water Tracers for Oil Field Applications. *Energy Fuel*. **2011**, *25*, 4488–4496.
- (3) Hutchins, R. D.; Dovan, H. T.; Sandiford, B. B. Aqueous Tracers for Oilfield Applications; *SPE International Symposium on Oilfield Chemistry, Anaheim, CA*, 1991.
- (4) Tayyib, D.; Al-Qasim, A.; Kokal, S.; Huseby, O. Overview of Tracer Applications in Oil and Gas Industry; *SPE Kuwait Oil & Gas Show and Conference, Mishref, Kuwait*, 2019.
- (5) Patidar, A. K.; Joshi, D.; Dristant, U.; Choudhury, T. A Review of Tracer Testing Techniques in Porous Media Specially Attributed to the Oil and Gas Industry. *J. Pet. Explor. Prod. Technol.* **2022**, *12*, 3339–3356.
- (6) Sanni, M.; Al-Abbad, M.; Kokal, S.; Dugstad, Ø.; Hartvig, S.; Huseby, O. Pushing the Envelope of Residual Oil Measurement: A Field Case Study of a New Class of Inter-well Chemical Tracers. *J. Petrol. Sci. Eng.* **2018**, *163*, 538–545.
- (7) Sanni, M. L.; Al-Abbad, M. A.; Kokal, S. L.; Hartvig, S.; Olaf, H.; Jevanord, K. A Field Case Study of Inter-well Chemical Tracer Test; *SPE International Symposium on Oilfield Chemistry, The Woodlands, TX*, 2015.
- (8) Chatterjee, M.; Toh, S.; Alshmakhy, A.; Bigno, Y.; Hewitt, P. In Advanced Research and Development in Unconventional Use of Tracer Technology for EOR and IOR: What Lies Beyond?; *Abu Dhabi International Petroleum Exhibition & Conference, Abu Dhabi, UAE*, 2021.
- (9) Khmelitskiy, V.; Aljabri, N.; Solovyeva, V. Fluorescent Based Tracers for Oil and Gas Downhole Applications: Between Conventional and Innovative Approaches. *Eng. Proc.* **2022**, *19*, 12.
- (10) Galdiga, C. U.; Greibrokk, T. Ultra-trace Determination of Fluorinated Aromatic Carboxylic Acids in Aqueous Reservoir Fluids using Solid-phase Extraction in Combination with Gas Chromatography–mass spectrometry. *J. Chromatogr. A* **1998**, *793*, 297–306.
- (11) Noviana, E.; Ozer, T.; Carrell, C. S.; Link, J. S.; McMahon, C.; Jang, I.; Henry, C. S. Microfluidic Paper-based Analytical Devices: From Design to Applications. *Chem. Rev.* **2021**, *121*, 11835–11885.
- (12) Gong, M. M.; Sinton, D. Turning the Page: Advancing Paper-based Microfluidics for Broad Diagnostic Application. *Chem. Rev.* **2017**, *117*, 8447–8480.
- (13) Yang, Y.; Noviana, E.; Nguyen, M. P.; Geiss, B. J.; Dandy, D. S.; Henry, C. S. Paper-based Microfluidic Devices: Emerging Themes and Applications. *Anal. Chem.* **2017**, *89*, 71–91.
- (14) Cate, D. M.; Adkins, J. A.; Mettakoonpitak, J.; Henry, C. S. Recent Developments in Paper-based Microfluidic Devices. *Anal. Chem.* **2015**, *87*, 19–41.
- (15) Ow, H.; Chang, S.; Thomas, G.; Shi, R.; Wang, W.; Chen, H.; Poitzsch, M. E.; Abdel-Fattah, A. First Deployment of a Novel Advanced Tracers System for Improved Waterflood Recovery Optimization; *Abu Dhabi International Petroleum Exhibition & Conference, Abu Dhabi, UAE*, 2018.
- (16) Thomas, G.; Ow, H.; Chang, S.; Shi, R.; Wang, W.; Chen, H.; Poitzsch, M.; Shateeb, H.; Abdel-Fattah, A. Deployment and Detection of a Novel Barcoded Advanced Tracers System for the Optimization of Improved Waterflood Recovery in Hydrocarbon Reservoirs; *SPE Middle East Oil and Gas Show and Conference, Manama, Bahrain*, 2019.
- (17) Shi, R.; Ow, H.; Thomas, G. M.; Chang, S.; Chen, H.; Wang, W.; Yoon, B. Zwitterionic Dipicolinic Acid-based Tracers for Reservoir Surveillance Application. *Ind. Eng. Chem. Res.* **2021**, *60*, 17804–17813.
- (18) Chen, H.; Shi, R.; Ow, H. Predicting Stability Constants for Terbium(III) Complexes with Dipicolinic Acid and 4-Substituted Dipicolinic Acid Analogues using Density Functional Theory. *ACS Omega* **2019**, *4*, 20665–20671.
- (19) Ow, H.; Chang, S.; Thomas, G.; Wang, W.; Mashat, A. A.; Shateeb, H. Automatable High Sensitivity Tracer Detection: Toward Tracer Data Enriched Production Management of Hydrocarbon Reservoirs; *SPE Annual Technical Conference and Exhibition, Dubai, UAE*, 2021.

- (20) Chang, S.; Thomas, G.; Wang, W.; Ow, H. Fully Automated Microfluidic Mixing Aided In-line Detection of Trace Level Oil Field Tracers. *Geoenviron. Sci. Eng.* **2023**, *222*, No. 111171.
- (21) Hindle, A. A.; Hall, E. A. H. Dipicolinic acid (DPA) Assay Revisited and Appraised for Spore Detection. *Analyst* **1999**, *124*, 1599–1604.
- (22) Bhardwaj, N.; Bhardwaj, S.; Mehta, J.; Kim, K.-H.; Deep, A. Highly Sensitive Detection of Dipicolinic Acid with a Water-dispersible Terbium-metal Organic Framework. *Biosens. Bioelectron.* **2016**, *86*, 799–804.
- (23) Cable, M. L.; Kirby, J. P.; Levine, D. J.; Manary, M. J.; Gray, H. B.; Ponce, A. Detection of Bacterial Spores with Lanthanide–Macrocyclic Binary Complexes. *J. Am. Chem. Soc.* **2009**, *131*, 9562–9570.
- (24) Cable, M. L.; Kirby, J. P.; Sorasaene, K.; Gray, H. B.; Ponce, A. Bacterial Spore Detection by  $[\text{Tb}^{3+}(\text{macrocyclic})(\text{dipicolinate})]$  Luminescence. *J. Am. Chem. Soc.* **2007**, *129*, 1474–1475.
- (25) Rosen, D. L.; Sharpless, C.; McGown, L. B. Bacterial Spore Detection and Determination by Use of Terbium Dipicolinate Photoluminescence. *Anal. Chem.* **1997**, *69*, 1082–1085.
- (26) Pu, S.; Shi, C.; Lv, C.; Xu, K.; Hou, X.; Wu, L.  $\text{Tb}^{3+}$ -based Off–On Fluorescent Platform for Multicolor and Dosage-sensitive Visualization of Bacterial Spore Marker. *Anal. Chem.* **2023**, *95*, 8137–8144.
- (27) Kovacs, D.; Kiraev, S. R.; Phipps, D.; Orthaber, A.; Borbas, K. E. Eu(III) and Tb(III) Complexes of Octa- and Nonadentate Macrocyclic Ligands Carrying Azide, Alkyne, and Ester Reactive Groups. *Inorg. Chem.* **2020**, *59*, 106–117.
- (28) Boltersdorf, T.; Gavins, F. N. E.; Long, N. J. Long-lived Lanthanide Emission via a pH-Sensitive and Switchable LRET Complex. *Chem. Sci.* **2021**, *12*, 8740–8745.
- (29) Parker, D.; Fradgley, J. D.; Wong, K.-L. The Design of Responsive Luminescent Lanthanide Probes and Sensors. *Chem. Soc. Rev.* **2021**, *50*, 8193–8213.
- (30) Pershagen, E.; Nordholm, J.; Borbas, K. E. Luminescent Lanthanide Complexes with Analyte-Triggered Antenna Formation. *J. Am. Chem. Soc.* **2012**, *134*, 9832–9835.
- (31) Fisher, C. M.; Fuller, E.; Burke, B. P.; Mogilireddy, V.; Pope, S. J. A.; Sparke, A. E.; Déchamps-Olivier, I.; Cadiou, C.; Chuburu, F.; Faulkner, S.; Archibald, S. J. A Benzimidazole Functionalised DO3A Chelator showing pH Switchable Coordination Modes with Lanthanide Ions. *Dalton T.* **2014**, *43*, 9567–9578.
- (32) Delgado-Pinar, E.; Albelda, M. T.; Frías, J. C.; Barreiro, O.; Tejera, E.; Kubiček, V.; Jiménez-Borreguero, L. J.; Sánchez-Madrid, F.; Tóth, É.; Alarcón, J.; García-España, E. Lanthanide Complexes as Imaging Agents Anchored on Nano-sized Particles of Boehmite. *Dalton T.* **2011**, *40*, 6451–6457.
- (33) Delgado-Pinar, E.; Frías, J. C.; Jiménez-Borreguero, L. J.; Albelda, M. T.; Alarcón, J.; García-España, E. One-pot Preparation of Surface Modified Boehmite Nanoparticles with Rare-earth Cyclen Complexes. *Chem. Commun.* **2007**, 3392–3394.
- (34) Carron, S.; Bloemen, M.; Vander Elst, L.; Laurent, S.; Verbiest, T.; Parac-Vogt, T. N. Ultrasmall Superparamagnetic Iron Oxide Nanoparticles with Europium(III) DO3A as a Bimodal Imaging Probe. *Chem. – Eur. J.* **2016**, *22*, 4521–4527.
- (35) Moadhen, A.; Elhouichet, H.; Jardin, C.; Oueslati, M.; Roger, J. A. Cathodoluminescent Properties of Tin Dioxide Sol–gel Doped with  $\text{Tb}^{3+}$  and  $\text{Eu}^{3+}$  grown in Porous Silicon. *phys. status solidi A* **2005**, *202*, 1508–1512.